Journal of Archaeological Science 52 (2014) 524–534

Contents lists available at ScienceDirect

Journal of Archaeological Science

journal homepage: http://www.elsevier.com/locate/jas

# Chronology of the Middle Palaeolithic open-air site of Combe Brune 2 (Dordogne, France): a multi luminescence dating approach

Marine Frouin [a, *], Christelle Lahaye [a], Marion Hernandez [a], Norbert Mercier [a], Pierre Guibert [a], Michel Brenet [b, c], Milagros Folgado-Lopez [b, c], Pascal Bertran [c, d]

[a] Institut de Recherche sur les Archéomatériaux – Centre de Recherche en Physique Appliquée à l'Archéologie (IRAMAT-CRP2A, UMR 5060), Université Bordeaux – Montaigne – CNRS, 33607 Pessac cedex, France
[b] INRAP, Pôle mixte de recherche, domaine de Campagne, 24260 Campagne, France
[c] PACEA, UMR 5199 Université Bordeaux 1 – CNRS, bâtiment B18, 33405 Talence cedex, France
[d] INRAP, Centre d'activité les Échoppes, 156 avenue Jean Jaurès, F-33600 Pessac, France

ARTICLE INFO

*Article history:*
Received 7 January 2014
Received in revised form
11 September 2014
Accepted 15 September 2014
Available online 22 September 2014

*Keywords:*
OSL
IRSL
Post-IRSL
TL
Dating
Early Middle Palaeolithic
Open-air site

ABSTRACT

The Bergerac region of south-western France is well known for its wealth of Middle Palaeolithic open-air sites. However, their chronology remains poorly understood due to the complexity of the deposits and difficulties applying radiometric dating techniques. Combe Brune 2, excavated in 2006 and 2007 by the INRAP (*Institut National de Recherches Archéologiques Préventives*), comprises a substantial stratigraphic sequence providing an almost continuous sedimentary record that is unique for the region. Three lithic assemblages were documented in the eastern part of the site and six stratified assemblages in the western part, five of which are concentrated in Unit 7. All the clearly individualised industries portray an unequivocal techno-economic coherence and are dominated by Levallois debitage.

Minerals present in the sediments were dated by the Optically Stimulated Luminescence (OSL) using different protocols (Thermal–Transfer: TT-OSL for quartz grains and IRSL and post-IR IRSL for feldspar grains). Heated flints were also dated by thermoluminescence (TL). Dating results obtained from quartz and feldspars grains provide an age of 234 ± 25 ka for Unit 8 at the base of the western sequence, 161 ± 18 to 97.3 ± 12 ka for Unit 7; 63.1 ± 6.5 ka for Unit 4 and a series of ages ranging from 39.2 ± 4.0 to 22.3 ± 2.2 ka for Unit 3. TL ages obtained from heated flints recovered from the base of Unit 7 in the eastern section range from 183 ± 20 to 195 ± 16 ka. These results are in good agreement and are stratigraphically coherent, suggesting that the Early Middle Palaeolithic occupation, the first documented for the Bergerac region, can be placed at the end of Marine Isotopic Stage (MIS) 7 and the beginning of MIS 6.



## 1. Introduction

Neanderthal lithic production concepts, methods and techniques portray substantial diversity from the beginning of the penultimate interglacial (MIS) 7) in south-western France. The archaeological record of the Bergerac area in the Dordogne region, and more precisely the Pécharmant limestone plateau, has produced a large number of Lower and Middle Palaeolithic sites (Brenet, 2011; Brenet et al., 2014). These occupations found in the same lithic raw material provisioning territory, all share particular economic and behavioural characteristics both in terms of production systems (debitage and *façonnage*) and associated tools.

Despite available lithostratigraphic and archaeostratigraphic data, it nevertheless remains difficult to discern the changing nature and function of these sites. This is particularly true of Middle Palaeolithic open-air given both their rarity and the fact that they are often less well-preserved in comparison to rock-shelters or cave sites. The open-air site of Combe Brune 2 differs from contemporary sites by 1) a thick, well-preserved sedimentary sequence permitting each lithic assemblage to be clearly individualised; 2) the presence of very diverse lithic artefacts, which provide insights for the *in situ* exploitation of local flint, including blank production

* Corresponding author. +33 6 29 59 98 33.
*E-mail addresses:* marine.frouin@u-bordeaux-montaigne.fr, marine.frouin@u-bordeaux3.fr (M. Frouin).

http://dx.doi.org/10.1016/j.jas.2014.09.012
0305-4403/

and/or transformation as well as the export of cores and blanks; and 3) the presence of heated lithic material.

Here we present dating results obtained from a combination of luminescence methods employing various materials (heated flint, quartz and feldspar grains). This new chronological framework makes possible a comparison of site-scale palaeoenvironmental data against regional palaeoclimatic patterns. Similarly, the chronological position of the Combe Brune 2 lithic assemblages is discussed with reference to other Early Middle Palaeolithic sites in the Bergerac area.

## 2. Combe Brune 2

The open-air site of Combe Brune 2, discovered during road works close to Bergerac (Fig. 1), lies on the edge of the Pécharmant limestone plateau, a few dozen metres south of Combe Brune 3 (Brenet, 2011). Following initial trench test pits in 2003, which produced evidence for several Middle Palaeolithic levels (Bourguignon et al., 2004), the site was excavated by an INRAP team directed by M. Brenet and M. Folgado between October 2006 and February 2007.

### 2.1. Morpho-geological context

Combe Brune 2 is located on a heavily karstified Cretaceous limestone plateau covered by flint-clays and discontinuous Tertiary alluvial sands and gravels. Two approximately 700 square metre areas were excavated. In the southeastern part of the site, the stratigraphy is compressed, with the archaeological level resting on a clast-supported gravel layer at the top of the flint–clay deposits (supplementary data S1). This layer, overlain by 0.6 m of loessic material, is interpreted as a Pleistocene coarse-grained lag deposit connected to the long-term alteration of the gravely clay. The undulating topography of the coarse-grained lag deposit documented during excavations was scattered with small depressions resulting from karstic subsidence. The western part of the site comprises two coalescent dolines infilled predominately with fine-grained colluvial sediments, which derive from the reworking of loessic material, together with local Tertiary sands and clayey weathering products (Fig. 2).

The stratigraphy of doline 2, from which most of the artefacts were recovered, is composed of nine units (from top to bottom):

- Unit 1 – Dark brown sandy silts, 35 cm thick (horizon *A*, plowsoil).
- Unit 2 – Dark yellow-brown clayey silts, 0–50 cm thick (horizon *Bw* in Holocene colluvium).
- Unit 3 – Light yellow-brown sandy silts, with Fe–Mn mottles and a sub-angular blocky structure, 0–35 cm thick (horizon *Eg*).
- Unit 4 – Brown-yellow (10 YR) compact clayey silts with Fe–Mn mottles, 60–120 cm thick (glossic horizon *Bt*). Units 3 and 4 correspond to a Holocene luvisol in loessic colluvium.
- Unit 5 – Brown-yellow sandy silts with scattered small gravels and a sub-angular blocky structure, 0–20 cm thick. Rounded Fe–Mn concretions are abundant (horizon *Bir*).
- Unit 6 – Bright brown (7.5 YR) clayey silts with a platy structure, 60 cm (horizon *IIBt* in a Pleistocene luvisol containing with loessic colluvium).
- Unit 7 – Heavily mottled, sandy silts with a prismatic structure, 50 cm (gleyic horizon *IIBg*). The main artefact-bearing horizon was found in this unit.
- Unit 8 – Red-brown (5 YR) sandy clays with a prismatic structure (*IIIBt* horizon of a Pleistocene luvisol).
- Unit 9 – Sandy gravel with a red, clayey matrix and a few sandstone blocks (colluviated Tertiary alluvium).

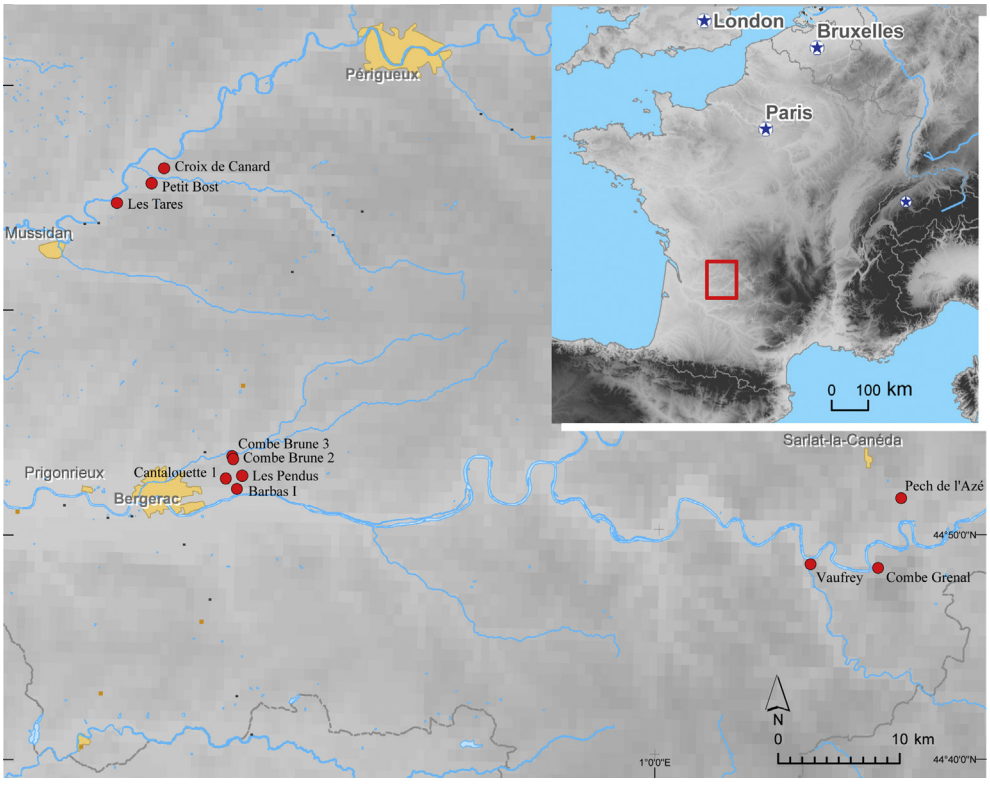


**Fig. 1.** Location of Combe Brune 2 and Early Middle Palaeolithic sites mentioned in the text.

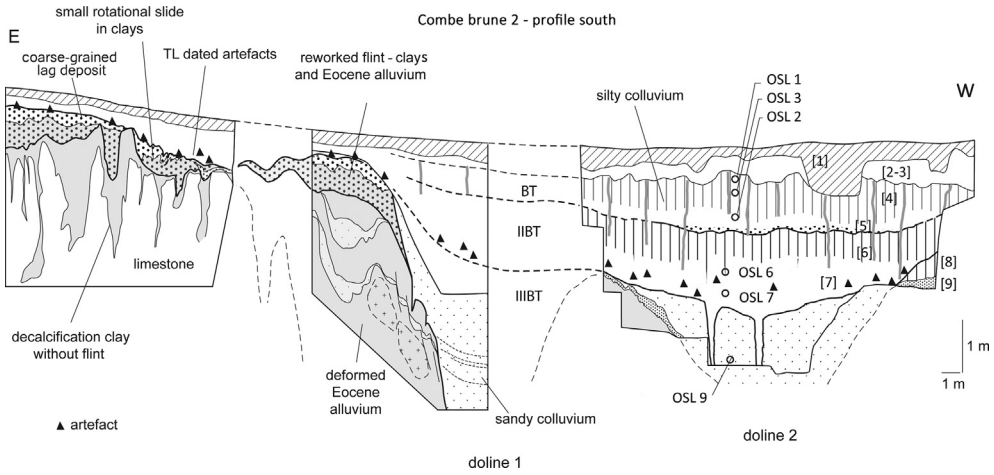


**Fig. 2.** General stratigraphic section of the site and distribution of the archaeological material. Unit numbers are indicated in brackets.

### 2.2. Lithic assemblages

Lithic assemblage VIIb (Fig. 3, colour figure in supplementary data S.2) was recovered from the heavily eroded eastern sector in a very dense deposit embedded above the residual stony layer (Brenet et al., 2008). Comprising more than 4500 lithic artefacts, the industry is characterised primarily by Levallois debitage (supplementary data S.3) with a fairly pronounced laminar tendency. Sought-after end products comprise various morphologies, including elongated or pointed forms. Discoid debitage producing more robust, often sub-triangular, backed blanks is also present, although in significantly smaller proportions (Brenet, 2013). While certain blocks show evidence for the production of large flakes according to an alternating platform technique (Ashton, 1992), others show a possible passage between the Levallois and Discoid methods. Blanks and prepared cores intended for later uses were exported from the site, and flake tools are not very abundant, primarily denticulates and Levallois points. Particular macro-tools on naturally fractured flint fragments (geofacts) and several shaped (*façonnage*) artefacts were also found in areas where the occupations were in direct proximity to an abundant raw material source. This zone could represent a mixed activity area associated with both the production of blanks partly intended for export and the less important use of a variety of different tools.

In the western area, six stratified lithic assemblages were identified: Level VIII in Unit 8; Levels X, VIIa, VI, V, and II at the base of Unit 7, and Level II sup. at the base of Unit 4. These distinct assemblages (Fig. 3) portray a clear techno-economic coherence and are all dominated by the Levallois method (Fig. 4). Sought-after end products are represented by elongated and/or triangular blanks that are morphologically similar to Levallois points, and Discoid debitage is present in the form of typical backed (*débordant*) products. The presence of very robust bifacial pieces and blocks portraying evidence for both debitage and shaping (*façonnage*) in levels VIII, X, and VIIa is also noteworthy. While the assemblages from levels VI and V could correspond to remnants of episodic knapping clusters, the others are characterised by incomplete debitage phases with several imported or exported artefacts and a flake tool component that is sometimes more abundant than in the eastern area. In the upper part of both sequences (Level I in the eastern area and Level II sup. in the western area), the presence of several bifacial pieces would indicate more recent occupations or

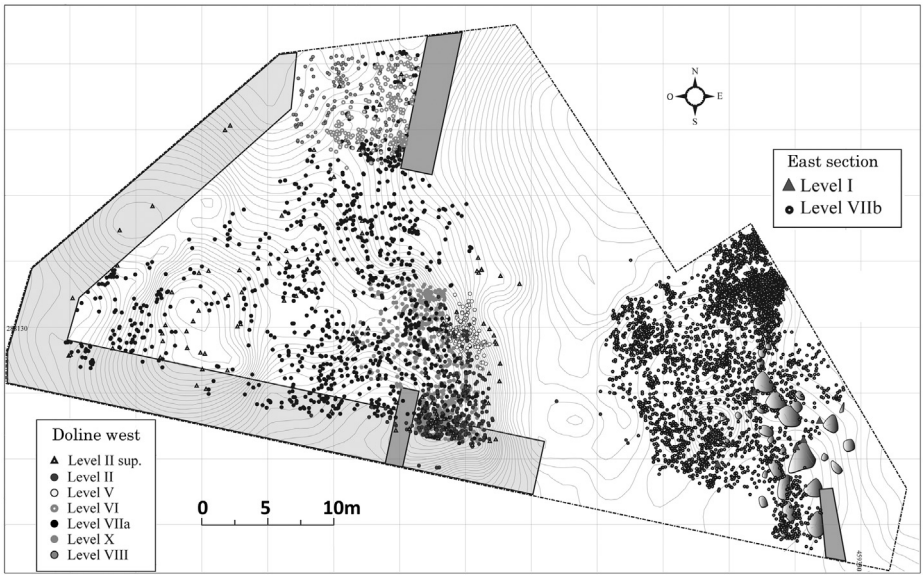


**Fig. 3.** Distribution of the lithic remains.

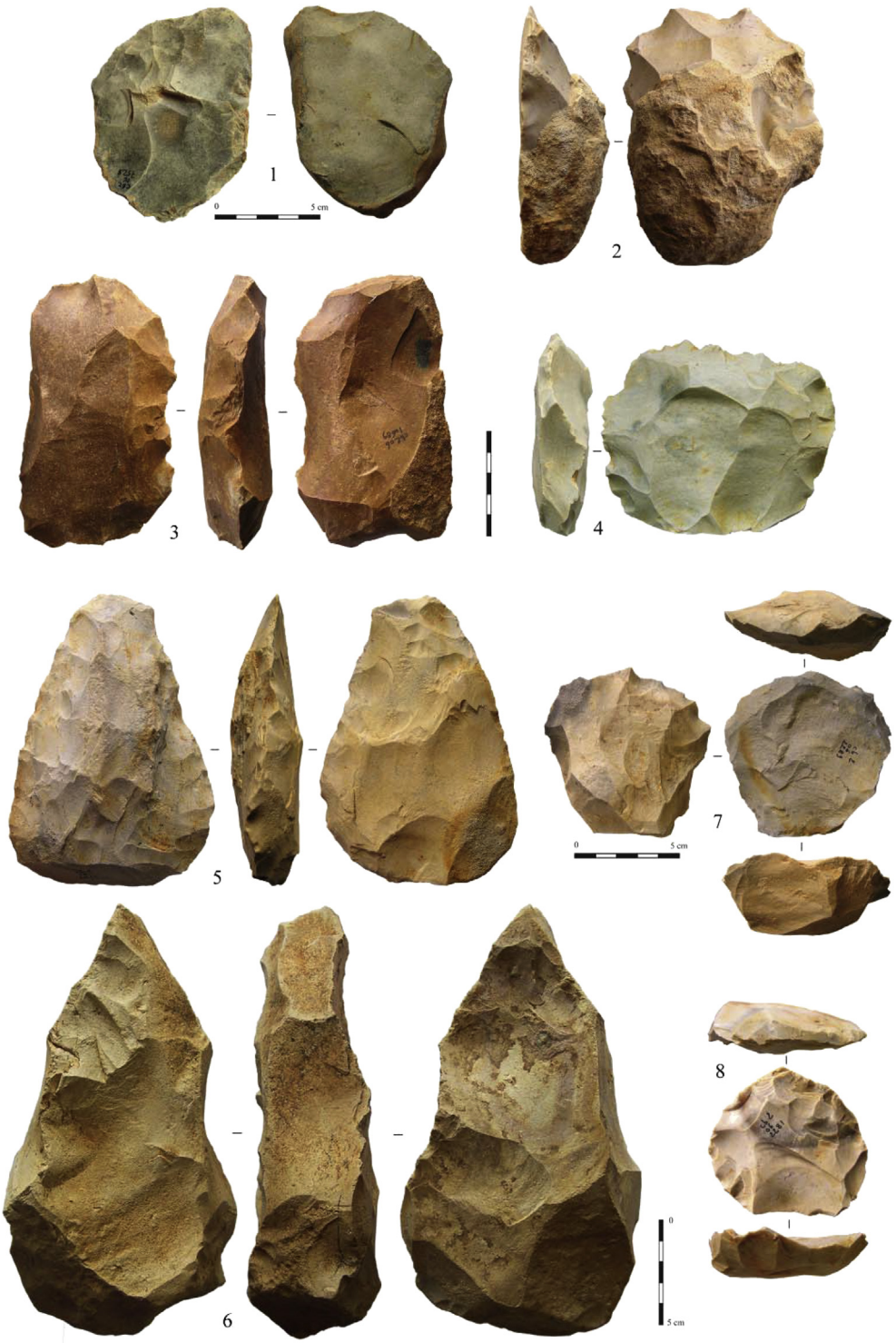


**Fig. 4.** Examples of the Combe Brune 2 lithic industry for level VIII, Unit 8: macro-denticulate (1) and core recycled as a side scraper (2); level X: laminar Levallois core (3) and centripetal Levallois core (4); level VIIa: biface (5) and knapped and shaped (*façonnage*) block (6); level II: Levallois cores recycled as tools (7 and 8). *(photos by M. Folgado).*

passages. Moreover, their exceptional preservation suggests these pieces to have been rapidly buried by short accumulation events. These small lithic assemblages most likely represent specialised activities tied to the use of bifacial tools made elsewhere and imported to the site (Claud, 2008). The morpho-technological characteristics of these bifacial pieces portray interesting comparisons with the region's other Late Middle Palaeolithic lithic assemblages with a bifacial component, such as the one from the nearby site of Combe Brune 1 attributed to the MTA (Mousterian of Acheulean Tradition; Bourguignon et al., 2012).

## 3. Materials and methods

The presence of heated flint artefacts and the abundance of minerals such as quartz and feldspar throughout the stratigraphic sequence were ideal for the application of luminescence dating

techniques. While the interest of dating heated flints, which can be directly connected to anthropic activity, is clear (e.g. Mercier, 1991; Mercier et al., 1995a,b; Tribolo, et al., 2009; Valladas et al., 2007, Valladas et al., 2001, Valladas et al., 2003; Richter et al., 2012), the lack of sufficient quantities of suitable samples often precludes applying thermoluminescence techniques. On the other hand, sedimentary quartz and feldspars are common on both enclosed and open-air sites, at least in the region considered here. Bearing this in mind, in order to produce a robust chronology for Combe Brune 2, we have combined direct TL dates on heated artefacts, considered clear proxies of anthropic activity, with OSL and IRSL dates on quartz and feldspar. The latter provide a chronological framework for the depositional sequence, and thus indirectly date the human occupations (e.g. Mercier et al., 2003, Mercier et al., 2007, Guérin et al., 2012).

Several field visits between November 2006 and January 2007 were necessary to collect the various samples. Sediments destined for OSL and IRSL determinations were sampled in the main levels of the western sector by inserting opaque metallic cylinders (Ø ≈ 4 cm) into cleaned sections. The cylinders were sealed immediately following retrieval. Samples were collected from Unit 3 (top: OSL1, wedge cast: OSL3), Unit 4 (OSL2), Unit 7(top: OSL6, base: OSL7), and at the base of Unit 8 (OSL 9). Sediment sample OSL7 also marks the top of the artefact bearing level recorded in the site's western section. Only rubified flints with potlids were selected for TL dating, among which, only twelve were sufficiently large and homogeneous. However, suitability tests revealed only one-third to have been sufficiently heated in the past. These 4 samples (Bdx 11153, 11154, 11156, 11164) come from the eastern sector above the weathering products and the residual stony layer at the base of Unit 7. Additional sediment samples were also taken in this area for dosimetric measurements in the laboratory.

### 3.1. Determination of the annual dose rate

The annual dose rate was determined as the per-year sum of absorbed ionizing radiation (alpha, beta, and gamma) emitted by decaying radioelements in the surrounding sediments and by cosmic rays. While the internal dose contribution of radioelements present in flint or K-feldspar must also be accounted for, the internal dose can be considered negligible for quartz given it contains low quantities of radioelements (~1 p.p.b, i.e. 0.001 μg/g).

Alpha and beta doses for the quartz and feldspar grains were calculated from the radioelement (K, U, and Th) content of the sediment samples, which was measured using low-background gamma spectrometry (Guibert and Schvoerer, 1991; Guibert et al., 2009) and taking into account grain-size sensitive attenuation factors (Mejdahl, 1979; Brennan et al., 1991; Fain et al., 1999). The internal K content for K-feldspar grains was assumed to be 12.5 ± 0.5% (Huntley and Baril, 1997). Similarly, the internal dose rate of the dated flints was calculated from their radioelement contents.

The external dose rate received by all the samples was also calculated from the radioelement content of the surrounding sediments, with the cosmic contribution estimated by taking into account burial depth as well as the site's latitude and altitude (Prescott and Hutton, 1994). The water content of each sample was measured in the laboratory and assumed to approximate the average value throughout the burial period.

### 3.2. Equivalent dose determination

Sediment samples were prepared according to well-established protocols (Wintle, 1997). Laser granulometry was used to measure particle-size distribution and identify the dominate fraction in the sediment samples. The coarse silt fraction (20–60 μm) was the most abundant in the six sediment samples and was therefore selected for OSL/IRSL measurements. This fraction was treated with hydrochloric acid (10% HCl) followed by hydrogen peroxide (30% $H_2O_2$) for 24 h in order to remove carbonates and organic matter, respectively. Considering the small quantities of material available, the 20–41 μm polymineral fraction rich in K-feldspars was selected for IRSL measurements. An additional weeklong treatment with a mixture of hexafluorosilicic (30% $H_2SiF_6$) and nitric ($HNO_3$) acids was used to isolate the quartz component of the 41–60 μm fraction by dissolving the feldspar and feldspathoid grains.

The outer 2 mm of the surface exposed to alpha and beta radiations were removed from the heated flints retained for TL measurements, with the remaining portion ground into a sub-200 μm powder (Tribolo et al., 2009). The 80–200 μm fraction was separated by dry sieving and subsequently subjected to conventional HCl and $H_2O_2$ treatments.

After rinsing, drying, and sieving, the 20–41 μm polymineral fraction was gently settled on aluminium disks by decantation (~1 mg), made to adhere to the disks with silicone spray for the 41–60 μm quartz fraction (~2 mg), or simply placed in brass cups in the case of the flint powder. These disks/cups were subsequently used for the luminescence experiments to determine the equivalent dose of each sample. The <40 μm granulometric fraction of the flint samples was used to determine the k-value, which represents the relative alpha-efficiency (with respect to beta particles) to produce luminescence (Aitken, 1985).

Luminescence measurements were performed using two Risø TL/OSL DA-15 readers (Bøtter-Jensen et al., 2003) equipped with $^{90}Sr/^{90}Y$ sources delivering 0.165 Gy $s^{-1}$ dose rate to the fine polymineral grains (20–41 μm) and a 0.160 Gy $s^{-1}$ dose rate to the 41–60 μm quartz fraction. The feldspar luminescence signals were stimulated using infra-red LEDs (850 ± 50 nm) were filtered through a combination of optical filters (Corning type 7-59/Schott BG39) and detected with a photomultiplier tube (EMI 9235 QA). Similarly, the OSL stimulation of quartz was induced by blue LEDs (NICHIA type NSPB-500AS: 470 nm ± 30 nm) and the resulting signals selected by a combination of Schott GG420 and Hoya U-340 filters. The TL signals of the flints were measured with a specially-designed TL reader (patent ANVAR-CNRS, 1974; Schvoerer et al., 1975; Duttine et al., 2005).

## 4. Results

### 4.1. Annual dose

Radioelement content was measured using low-background gamma spectrometry, and associated dose rates were calculated using the method developed by Guérin and Mercier (2011, Tables 1 and 2).

Sediments samples from the upper two-thirds of the sequence in the western part of the site yielded a relatively consistent dose rate, ranging from 3.22 ± 0.11 Gy/ka for OSL 2 at the top to 3.76 ± 0.13 Gy/ka for OSL 6 in the lower part. The two samples from lower in the sequence (OSL 7 and OSL 9) do, however, show much lower radioelement contents (twice as low on average). Although the reason for these differences is not known, it is highly unlikely that they are linked to any recent radioelement leaching as the gamma spectrometry indicates similar $^{226}Ra$ and $^{238}U$ activity, and hence no significant U–Th disequilibrium (Fig. 5). The relatively low radioelement content of the lower horizons thus appears directly connected to the nature of the sediments.

K, U, and Th content of the sediments associated with the four heated flints from archaeological level 7 in the eastern part of the

**Table 1**
Dosimetric data for the sediment samples. Dose-rates calculated from the K, U and Th concentrations take into account the water content measured in the sediments.

| Sample | Sediment | | | | | | | | Feldspar | | | | | | | | | | Quartz | |
|---|---|---|---|---|---|---|---|---|---|---|---|---|---|---|---|---|---|---|---|---|
| | K | | U ($^{238}$U) | | U ($^{226}$Ra) | | Th | | Alpha | | Beta ext. | | Gamma | | Cosmic (Gy/ka) | Total | | | Total | |
| | (%) | σ | (eq. ppm) | σ | (eq. ppm) | σ | (ppm) | σ | (Gy/ka) | σ | (Gy/ka) | σ | (Gy/ka) | σ | | (Gy/ka) | σ | | (Gy/ka) | σ |
| OSL 1 | 1.12 | 0.02 | 3.86 | 0.17 | 3.91 | 0.05 | 14.6 | 0.15 | 0.58 | 0.12 | 1.50 | 0.02 | 1.20 | 0.01 | 0.22 | 3.61 | 0.12 | | 3.08 | 0.04 |
| OSL 3 | 0.99 | 0.03 | 3.54 | 0.17 | 3.60 | 0.05 | 13.6 | 0.15 | 0.53 | 0.11 | 1.36 | 0.02 | 1.11 | 0.01 | 0.20 | 3.31 | 0.12 | | – | – |
| OSL 2 | 0.95 | 0.02 | 3.69 | 0.17 | 3.32 | 0.04 | 13.8 | 0.14 | 0.52 | 0.11 | 1.30 | 0.01 | 1.08 | 0.01 | 0.20 | 3.22 | 0.11 | | – | – |
| OSL 6 | 1.21 | 0.02 | 3.82 | 0.17 | 4.18 | 0.05 | 15.0 | 0.15 | 0.60 | 0.13 | 1.60 | 0.02 | 1.26 | 0.01 | 0.18 | 3.76 | 0.13 | | 3.21 | 0.04 |
| OSL 7 | 0.66 | 0.02 | 2.12 | 0.12 | 2.20 | 0.03 | 8.8 | 0.10 | 0.34 | 0.08 | 0.87 | 0.02 | 0.71 | 0.01 | 0.17 | 2.21 | 0.07 | | 1.85 | 0.03 |
| OSL 9 | 0.46 | 0.02 | 1.94 | 0.11 | 1.70 | 0.03 | 6.7 | 0.08 | 0.26 | 0.06 | 0.64 | 0.01 | 0.53 | 0.01 | 0.16 | 1.71 | 0.06 | | – | – |

**Table 2**
Dosimetric data for the heated flints.

| Sample | Flint | | | | | | | | | | | | | | | | | | | |
|---|---|---|---|---|---|---|---|---|---|---|---|---|---|---|---|---|---|---|---|---|
| | K | | U ($^{238}$U) | | U ($^{226}$Ra) | | Th | | | | Alpha int. | | Beta int. | | Beta ext. | | Gamma and cosmic | | Total | |
| | (%) | σ | (eq. ppm) | σ | (eq. ppm) | σ | (ppm) | σ | k | σ | (Gy/ka) | σ | (Gy/ka) | σ | (Gy/ka) | σ | (Gy/ka) | σ | (Gy/ka) | σ |
| BDX 11153 | 0.02 | 0.01 | 1.17 | 0.27 | 0.26 | 0.03 | 0.58 | 0.11 | 0.08 | 0.01 | 0.14 | 0.03 | 0.11 | 0.02 | 0.09 | 0.01 | 0.85 | 0.02 | 1.19 | 0.08 |
| Sediment associated | 0.59 | 0.05 | 3.42 | 0.07 | 2.60 | 0.02 | 12.98 | 0.08 | – | – | – | – | – | – | – | – | – | – | – | – |
| BDX 11154 | 0.00 | 0.02 | 0.27 | 0.16 | 0.13 | 0.05 | 0.65 | 0.11 | 0.09 | 0.02 | 0.08 | 0.02 | 0.04 | 0.02 | 0.00 | 0.00 | 0.66 | 0.02 | 0.92 | 0.05 |
| Sediment associated | 0.09 | 0.01 | 2.03 | 0.05 | 1.92 | 0.01 | 5.73 | 0.04 | – | – | – | – | – | – | – | – | – | – | – | – |
| BDX 11156 | 0.02 | 0.01 | 0.29 | 0.09 | 0.23 | 0.02 | 0.47 | 0.05 | 0.10 | 0.01 | 0.10 | 0.01 | 0.06 | 0.01 | 0.05 | 0.01 | 0.71 | 0.01 | 0.81 | 0.07 |
| Sediment associated | 0.59 | 0.01 | 3.42 | 0.07 | 2.60 | 0.02 | 12.98 | 0.08 | – | – | – | – | – | – | – | – | – | – | – | – |
| BDX 11164 | 0.01 | 0.02 | 0.25 | 0.40 | 0.25 | 0.40 | 0.00 | 0.50 | 0.07 | 0.01 | 0.05 | 0.09 | 0.05 | 0.06 | 0.00 | 0.01 | 0.81 | 0.02 | 0.90 | 0.16 |
| Sediment associated | 0.38 | 0.01 | 3.37 | 0.07 | 2.65 | 0.02 | 10.17 | 0.07 | – | – | – | – | – | – | – | – | – | – | – | – |

site are broadly similar and relatively close to those obtained for the same level in the western part (OSL 7). Not surprisingly, the radioelement content of the flints themselves is fairly low, revealing nearly 80% of the annual dose to come from external sources (beta, gamma and cosmic).

### 4.2. Equivalent dose

#### 4.2.1. Feldspars

Equivalent dose determinations for each disc covered with polymineral grains rich in K-feldspars was analysed according the SAR protocol (*Single Aliquot Regenerative Dose*; Auclair et al., 2003, Balescu et al., 2003). Apart from the first SAR cycle, each disc was irradiated by an artificial source and the IRSL signal measured. Characteristic growth curves describing variations in the IRSL signal were constructed by administering doses, and sensitivity changes were corrected for by introducing a constant test dose to each cycle.

Here we adopted the IRSL protocol proposed by Huntley and Lamothe (2001), hereafter referred to simply as $IR_{50}$, which comprises measuring the luminescence signals at 50 °C for 100 s after a 250 °C preheat for 60 s following each irradiation. An optical drainage (a 30 °C infrared stimulation for 300 s) was introduced at the end of each cycle to reset any residual signal before each regeneration step. The equivalent dose for each aliquot was estimated by interpolating the natural OSL signal onto the regeneration curve adjusted by an exponential function (see Fig. 6 for an example).

SAR equivalent dose measurements were verified with reference to the recycling ratio, which must be close to 1, and the recuperation ratio, which must remain as low as possible. For our samples, an average recycling ratio of 0.96 ± 0.20 and a recuperation ratio consistently less than 2% indicate, respectively, an effective correction of sensitivity changes and the absence of significant thermal transfer. The $IR_{50}$ mean equivalent dose for each sample at one sigma (Table 3) was calculated by averaging the measured doses from 6 aliquots.

Equivalent doses correction for anomalous fading (Wintle, 1973; Auclair et al., 2007; Wallinga et al., 2007), which results from

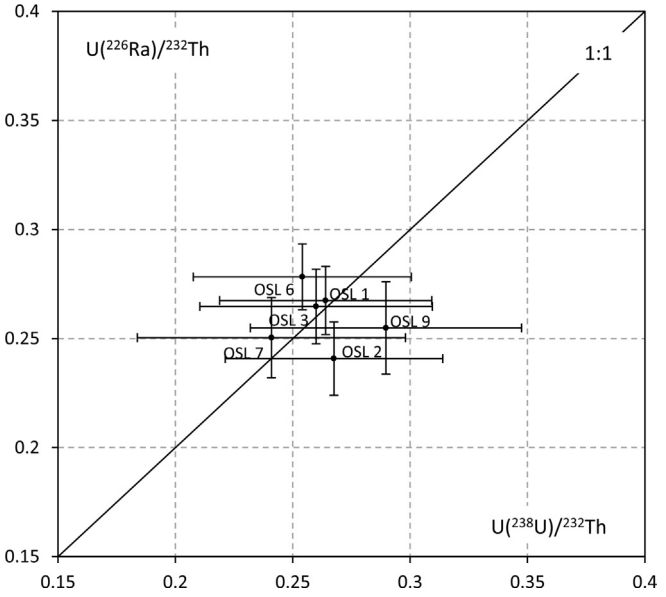


**Fig. 5.** Radioelement contents of the sediment samples. Measurements were performed in the IRAMAT-CRP2A laboratory using a "U-shaped", high resolution, low background gamma Ge detector (Eurisys Mesures, EGPC 200 P17).

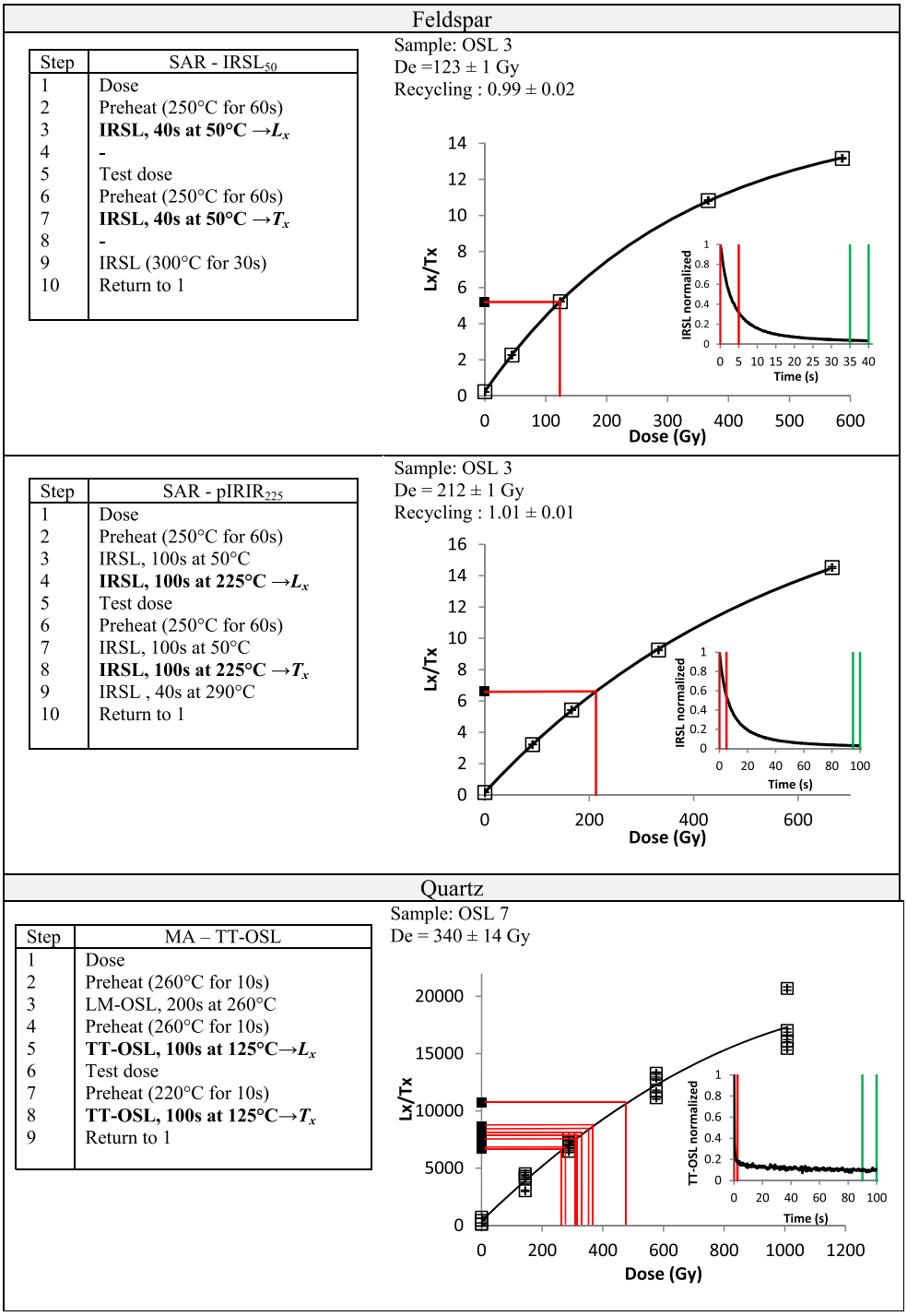


**Fig. 6.** Protocols for feldspar (SAR-IRSL$_{50}$ and SAR-pIR IR$_{225}$) and quartz (MA-TT-OSL) grains. In the case of feldspars, all growth curves were fitted with an exponential model (see sample OSL3 for an example), whereas for quartz a second order polynomial model was used. See text for more detail.

quantum-mechanical electron tunnelling (Visocekas, 1979) producing a constant leaching of charged particles accumulated by the crystal following irradiation, is necessary to avoid under-estimated ages. This correction is specific to each sample as the fading rate is linked to the more or less organised crystalline structure of feldspar (Spooner, 1994). As such, the fading rate was measured for each bleached disk by comparing the IRSL signal immediately following irradiation ($t = 0$) to the signal obtained after a defined interval. The decrease of the signal generates a straight line (when displayed on a logarithmic scale) whose slope corresponds to the fading rate, or "g value" (Aitken, 1985). However, fading experiments for three samples (OSL1, OSL2, and OSL3) showed the fading rate to be fairly low (~1%) for all samples. Consequently, an average rate of 1% was used for the other 3 samples (Table 3), with the ages corrected by applying the method outlined by Huntley and Lamothe (2001) for samples younger than ~50 ka and the DRC (*Dose-Rate Correction*) method (Lamothe et al., 2003) for older samples.

In addition to the IR$_{50}$ signal measurement, the post-IR-IRSL protocol at 225 °C (pIR IR$_{225}$) was tested since it necessitates little or no fading corrections (Thomsen et al., 2008; Morthekai et al.,

**Table 3**
Equivalent doses, fading rates, and calculated ages for the luminescence samples. The preferred ages have been highlighted in bold.

| Location | Sample | Feldspar | | | | | | | | | | | | Quartz | | | | Flint | | | |
|---|---|---|---|---|---|---|---|---|---|---|---|---|---|---|---|---|---|---|---|---|---|
| | | $D_e$ value[a] (Gy) | | | | g-value (%/decade) | | Fading uncorr. Age (ka) | | | | Fading corr. Age (ka) | | $D_e$ value (Gy) | | Age (ka) | | $D_e$ value (Gy) | | Age (ka) | |
| | | $IR_{50}$ | σ | pIR $IR_{225}$[b] | σ | $IR_{50}$ | σ | $IR_{50}$ | σ | pIR $IR_{225}$ | σ | $IR_{50}$ | σ | TT-OSL | σ | TT-OSL | σ | TL | σ | TL | σ |
| Unit 3 | OSL 1 | 77.6 | 1.6 | 94.9 | 4.1 | 0.95 | 0.10 | 21.5 | 2.4 | 26.2 | 3.0 | **22.3** | **2.2** | 56 | 8 | **18.2** | **3.0** | – | | – | |
| Unit 3 | OSL 3 | 120 | 2.6 | 148 | 6.2 | 1.09 | 0.10 | 36.2 | 4.1 | 44.7 | 5.2 | **39.2** | **4.0** | – | – | – | – | – | | – | |
| Unit 4 | OSL 2 | 189 | 4.9 | 204 | 8.6 | 1.17 | 0.10 | 58.7 | 6.7 | 63.4 | 7.4 | **63.1** | **6.5** | – | – | – | – | – | | – | |
| Unit 7 | OSL 6 | 366 | 8.9 | 366 | 14 | 1.00[c] | 0.10 | 97 0.3 | 11 | **97.3** | **12** | 149 | 14 | 379 | 21 | **118** | **13** | – | | – | |
| Unit 7 | OSL 7 | 331 | 8.2 | 356 | 16 | 1.00[c] | 0.10 | 150 | 16 | **161** | **18** | 193 | 20 | 340 | 14 | **184** | **19** | – | | – | |
| Unit 7 | BDX 11153 | – | | – | | – | | – | | – | | – | | – | | – | | 219 | 22 | **185** | **23** |
| Unit 7 | BDX 11154 | – | | – | | – | | – | | – | | – | | – | | – | | 145 | 10 | **183** | **20** |
| Unit 7 | BDX 11156 | – | | – | | – | | – | | – | | – | | – | | – | | 181 | 10 | **195** | **16** |
| Unit 7 | BDX 11164 | – | | – | | – | | – | | – | | – | | – | | – | | 169 | 7 | **187** | **21** |
| Unit 8 | OSL 9 | 353 | 9 | 400 | 16 | 1.00[c] | 0.10 | 207 | 22 | **234** | **25** | 263 | 27 | – | – | – | – | – | | – | |

[a] $D_e$ value is a weighted mean of measured aliquots.
[b] Residuals were subtracted from pIR $IR_{225}$ $D_e$ values.
[c] Fading rate is a weighted mean (1.0 ± 0.1) of measured aliquots from samples OSL 1, OSL 2 and OSL 3.

2008; Buylaert et al., 2009; Jain and Ankjaergaard, 2011). The pIR $IR_{225}$ equivalent doses were assessed for all the samples using a series of 6 aliquots (Table 3). Although the fading rate of the pIR $IR_{225}$ signal was not determined, it should be well below the 1% rate of the $IR_{50}$ signal, and thus was considered negligible. Moreover, resetting pIR $IR_{225}$ signals in feldspar grains is slower than the $IR_{50}$, which may contribute to the retention of some residual signal in pIR IR measurements (Buylaert et al., 2009). Separate aliquots were used to determine the post-bleaching residual doses: 0.6 ± 0.3 Gy (OSL1) to 1.1 ± 0.7 Gy (OSL9) for $IR_{50}$ and from 2.4 ± 0.2 Gy (OSL1) to 4.4 ± 0.3 Gy (OSL9) for pIR $IR_{225}$. The residual dose obtained for the $IR_{50}$ signal is always less than 1%, and was thus considered negligible. Based on the pIR $IR_{225}$ signal, the residual doses are less than or equal to 3% of the measured equivalent dose. Finally, the mean pIR $IR_{225}$ equivalent dose at one sigma (Table 3) was calculated for each sample as the average dose measured from 6 aliquots after subtracting the residual dose.

#### 4.2.2. Quartz

The most commonly accepted protocol for the OSL dating of quartz grains relies on the measurement of the fast component of the luminescence signal; however, this component saturates at a relatively low rate (~150–200 Gy), limiting the application of this method to the last 100 ka. As the assumed age of the deposits concerned here likely exceeds this threshold, we have adopted the TT-OSL protocol, which extends the age range of the OSL technique for quartz.

This protocol is based on the principle that quartz grains store charges in deep traps with a level of dose saturation at least three times higher than the fast component (Wang et al., 2006). In order to measure the TT-OSL signal, an initial preheat followed by an optical stimulation is necessary to empty traps associated with the fast component, followed by a second heating at 260 °C for 10 s, which induces the thermal transfer of charges in the deep traps towards those associated with the fast component.

An SAR-type protocol could not be implemented for measuring the TT-OSL signal to due sensitivity changes connected to repeated heating cycles (Hernandez et al., 2012). Consequently, a multiple aliquots (MA) protocol (Hernandez, 2011) was applied to three of the six sediment samples (OSL 1, 6, and 7). The growth curve of the dose-dependent TT-OSL signal was built from multiple aliquots, which were optically bleached in controlled laboratory conditions with a solar simulator (Fig. 6). Furthermore, 10 “natural” aliquots (not exposed to light or dosed) were measured for each sample, and the normalised intensity interpolated on the dose growth curve in order to determine the equivalent dose of each aliquot (mean equivalent doses provided in Table 3). The TT-OSL signals for any given regenerative dose are heavily dispersed, a pattern almost certainly tied to the varying behaviour of the grains present in each aliquot and which provides an indication as to the minimum dispersion observable with the natural signals.

#### 4.2.3. Flint

The multiple aliquot additive-regeneration dose method, or MAAR (Aitken, 1985), was adopted for determining equivalent doses of the flint samples. Several dozen aliquots of the naturally radiated material were measured with or without added doses and used to plot the first TL growth curve as a function of the added dose. For the second growth curve, a portion of the natural powder was first heated for 1 h at 400 °C followed by an additional hour at 500 °C in order to totally reset the TL signal before being subjected to artificial irradiation in the laboratory (Fig. 7). This thermal treatment is designed to produce the most homothetic luminescence curves possible, such that the luminescence dose response curves are similar in shape, for both the added and regenerated dose. Each sample was evaluated with a routine plateau test (Aitken, 1985) using a slide technique (Guibert et al., 1996). In the end, four samples satisfied the verification test and were retained for dating.

## 5. Results and discussion

### 5.1. Age determinations

The $IR_{50}$, pIR $IR_{225}$, TT-OSL, and TL results are all chronologically (Table 3) and stratigraphically coherent (Fig. 8). As anticipated, while the non-fading corrected $IR_{50}$ ages are always underestimated in respect to the pIR $IR_{225}$ ages, once corrected, the two sets are consistent, except for sample OSL6. This good agreement suggests that the feldspar grains had been well exposed to light before burial as the $IR_{50}$ and pIR $IR_{225}$ signals are known to bleach at different rates. In the case of sample OSL6, the uncorrected $IR_{50}$ age agrees well with the pIR $IR_{225}$ age, indicating that this sample does not require fading correction. As such, the pIR $IR_{225}$ ages of the samples that do not require correction are preferred. These ages are also in good agreement with the quartz TT-OSL ages obtained for sediment samples OSL1, 2, 6, and 7. Moreover, the pIR $IR_{225}$ and TT-OSL ages for sample OSL7 fall in the same age range as the TL ages

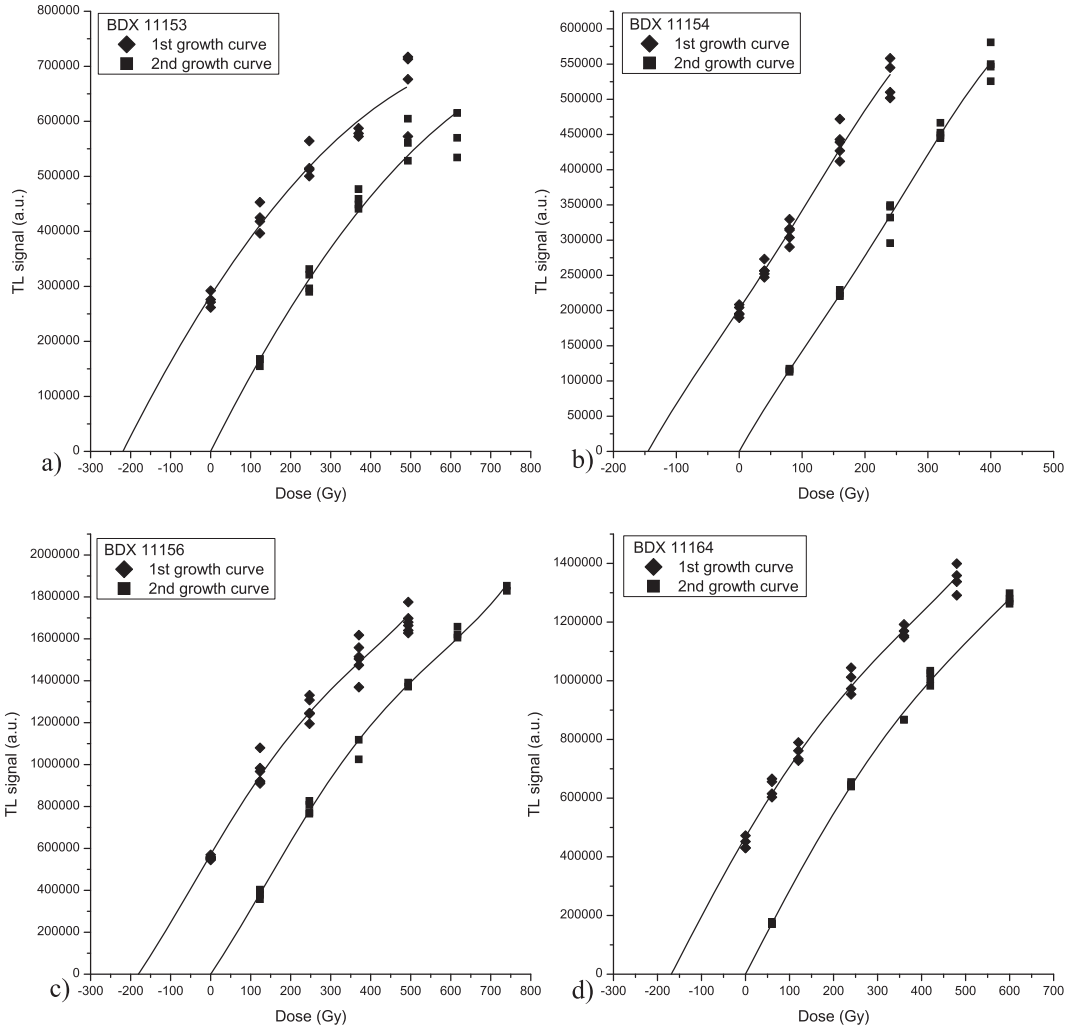


**Fig. 7.** First (additive dose) and second (regenerative dose) growth curves fitted with an exponential model for samples a) Bdx 11153; b) Bdx 11154; c) Bdx 11156; d) Bdx 11164.

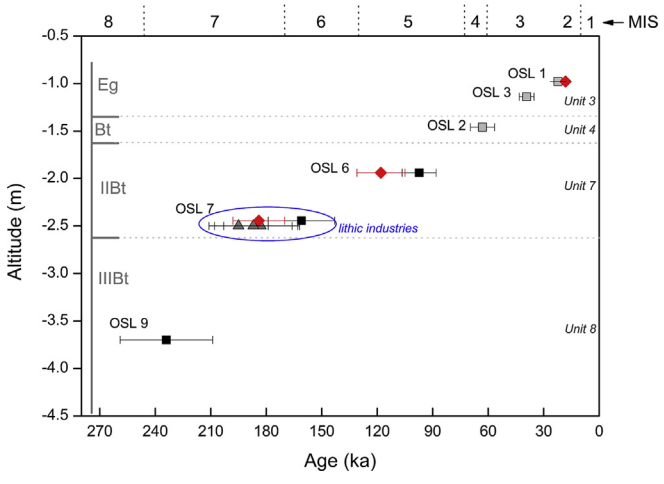


**Fig. 8.** Summary of the luminescence ages for Combe Brune 2. Gray triangles: TL ages of heated flints from the eastern sector. Squares: feldspars ages obtained for the western stratigraphic section; grey squares: $IR_{50}$ ages on feldspars for samples OSL2 and OSL3; solid squares: pIR $IR_{225}$ ages on feldspars. Red diamonds: TT-OSL ages on quartz grains from the western stratigraphic section. These ages correspond to the preferred values highlighted in bold in Tables 2 and 3.

and are consistent with the age of 234 ± 25 ka obtained for sample OSL9 from the bottom of the stratigraphic sequence, suggesting the burnt lithic pieces from the base of Unit 7 have not suffered any substantial post-depositional reworking.

### 5.2. Chronology and techno-economic behaviour

These new luminescence ages obtained for the Combe-Brune 2 complement available geomorphological data and shed light on the chronology of the region's Middle Palaeolithic lithic industries. The two main Middle Palaeolithic occupations in unit 7 of the eastern area form a palimpsest, and only the industry from the level attributed to the Early Middle Palaeolithic was found in the western area. While the pIR $IR_{225}$ results provide an age of ~160 ka (i.e. MIS6) for the level that yielded the Early Middle Palaeolithic industry, the fact that the MTA industry was documented solely in the eastern part precludes associating it with any of the age determinations.

If the interpretation of the residual stony layer at the base of the sequence is correct, the concentrations of objects attributed to the level VIIb would correspond to successive occupations of unknown duration and with little horizontal displacement of the artefacts. The presence of several MTA-type bifaces in level I clearly indicates that the stony layer was not significantly buried before the middle

of the Weichselian Pleniglacial. This absence of burial, indicative of a near-zero accumulation-erosion balance with the possibility of temporary accumulation of sediments followed by re-exhumation, implies that the archaeological level and the stony layer remained in the subsurface for some time. In this area, the archaeological level is therefore likely to correspond to the juxtaposition of several occupations of different ages. The TL dates obtained on the heated material from this palimpsest deposit provide ages that all range between 183 ± 20 and 195 ± 16 ka, or the end of MIS 7 and the very beginning of MIS 6. Moreover, these results are practically identical to the OSL and IRSL ages obtained in the western area for the Early Middle Palaeolithic level (Unit 7); making it reasonable to assumed that the four TL-dated flints all belong to this assemblage.

The infilling dynamics of the western doline are different; although affected horizontally and vertically by subsidence and colluviation phenomena, the individual archaeological levels would have been protected from erosion, buried individually, and separated by irregular periods of time similar to those deduced for the eastern area. In this sector, the archaeological levels are intercalated in the colluvial deposits and are consequently more likely to represent brief occupations. The IRSL ages obtained for the middle of Unit 8 suggest that this palaeosol developed during the penultimate interglacial (MIS 7). The IIBt horizon (Unit 6) that shows a complex structure at the microscopic scale with at least two phases of clay illuviation separated by a phase of deep seasonal frost (see Brenet et al., 2008) represents the first interglacial palaeosol below the Holocene soils. Given the dates obtained for the upper (Unit 4) and lower (Unit 7) levels, a broadly Eemian age (MIS 5) can be proposed for the IIBt horizon. Comparisons with well-dated loess sequences also shows that MIS 5 in Northern France sees the development of similar soil complexes (Van Vliet-Lanoë, 1990; Haessaerts et al., 1999; Antoine et al., 2003). Finally, the upper Bt horizon (Unit 4) corresponds to the Holocene luvisol.

The general interpretation of the site's lower levels sees a succession of occupations from the end of MIS 7 to the beginning of MIS 6 that, although spread across the entire surface, are differentially preserved in the eastern and western sectors of the site. Each of these occupations, regardless their duration or extent, show the recurrent use of the local raw material, especially in the eastern part where abundant high-quality flint was easily accessible in the flint–clay deposits. More diversified production sequences, sometimes involving tool use or transformation, were carried out towards the west (Brenet, 2011). Several recently studied Early Middle Palaeolithic industries from open-air sites in the Bergerac region have similarly been dated to MIS 7 or MIS 6 (Fig. 1). However, the lithic assemblages from Combe Brune 2 differs from contemporary assemblages in the Dordogne region, the Pécharmant plateau, or the Isle Valley given the still unique association of the alternating platform technique, Discoid and Levallois debitage, bifacial shaping, and the combination of debitage and bifacial shaping on the same block (Brenet et al., 2014). Finally, the site's function is also exceptional in the association of evidence for exported cores and blanks for later use with on-site blank production (sometimes sequenced) on an abundant source of raw material, the use of flake tools, sometimes on naturally fractured flints, and a macro-tool kit.

## 6. Conclusion

Our detailed study of the open-air site of Combe Brune 2, incorporating geological and geomorphological data and radiometric dating techniques, demonstrates a succession of occupations across the entire excavated surface and a differential preservation between both studied areas. The combination of dates obtained from various materials (quartz and feldspar grains and heated flints) using different luminescence methods (TT-OSL, $IR_{50}$, pIR $IR_{225}$, and TL) provides a robust and detailed chronology for the formation of the archaeological levels. Our results demonstrate that the Early Middle Palaeolithic occupation of Combe Brune 2 took place between the end of MIS 7 and the beginning of MIS 6. The chronological position of these occupations and the characterisation of their original lithic industries shed new light on the Early Middle Palaeolithic settlement of the Bergerac region, where no site from this period had previously been identified.

## Acknowledgements

This work received financial support from the Aquitaine Region Council through the program entitled “La radioluminescence des feldspaths: un nouvel outil de datation des gisements archéologiques et des séquence quaternaires d’Aquitaine”. This work was also supported by the ANR – n°ANR-10-LABX-52.

## Appendix A. Supplementary data

Supplementary data related to this article can be found at http://dx.doi.org/10.1016/j.jas.2014.09.012.

## References

Aitken, M.J., 1985. Thermoluminescence Dating. Academic Press, London, p. 359.
Antoine, P., Bahain, J.J., Debenham, N., Frechen, M., Gauthier, A., Hatté, C., Limondin-Lozouet, N., Locht, J.L., Raymond, P., Rousseau, D.D., 2003. Nouvelles données sur le Pléistocène du nord du Bassin Parisien : les séquences loessiques de Villiers-Adam (Val d’Oise, France). Quaternaire 14, 219–235.
Auclair, M., Lamothe, M., Huot, S., 2003. Measurement of anomalous fading for feldspar IRSL using SAR. Radiat. Meas. 37, 487–492.
Auclair, M., Lamothe, M., Lagroix, F., Banerjee, S.K., 2007. Luminescence investigations of loess and tephra from halfway house section, Central Alaska. Quat. Geochronol. 2, 34–38.
Ashton, N., 1992. The high lodge flint industries. In: Ashton, N., Cook, J., Lewis, S.J., Rose, J. (Eds.), High Lodge. Excavations by G. de Sieveking, 1962-8 and J. Cook, 1988. British Museum Press, Londres, pp. 124–168.
Balescu, S., Lamothe, M., Mercier, N., Huot, S., Balteanu, D., Billard, A., Hus, J., 2003. Luminescence chronology of Pleistocene loess deposits from Romania: testing methods of age correction for anomalous fading in alkali feldspars. Quat. Sci. Rev. 22, 967–973.
Bøtter-Jensen, L., Wintle, A.G., McKeever, S.W.S., 2003. Optically Stimulated Luminescence Dosimetry. Elsevier, Amsterdam.
Bourguignon, L., Ortega, F., Sellami, F., Brenet, M., Grigoletto, F., Vigier, S., Daussy, A., Casgrande, F., 2004. Les occupations paléolithiques découvertes sur la section nord de la déviation de Bergerac : résultats préliminaires obtenus à l'issue des diagnostics. Bull. préhistoire Du. Sud-Ouest 11, 155–172.
Bourguignon, L., Ortega, I., Blaser, F., Bidard, P., Vigier, S., Rios Garaizar, J., Lenoble, E.A., Sellami, F., Guibert, P., Vieillevigne, E., 2012. Les niveaux paléolithiques de Combe Brune 1, (Creysse, Dordogne), Bergerac, R.N. 21 section nord. Rapport Final d'Opération. INRAP, SRA Aquitaine.
Brenet, M., Folgado, M., Vigier, S., Claud, E., Bertran, P., Lahaye, C., Vieillevigne, E., Guibert, P., Leroy, N., 2008. Etude inter-disciplinaire des niveaux paléolithiques de Combe Brune 2 (Creysse, Dordogne), Bergerac, R.N. 21 section nord. Rapport Final d'Opération. INRAP, SRA Aquitaine, p. 254.
Brenet, M., 2011. Variabilité et signification des productions lithiques au Paléolithique moyen ancien. L'exemple de trois gisements de plein-air du Bergeracois (Dordogne, France). Université de Bordeaux 1, Bordeaux, p. 485.
Brenet, M., Bourguignon, Colonge, D., Folgado, M., Jarry, M., Lelouvier, L.-A., Mourre, V., Turq, 2014. Les techno-complexes au début du Paléolithique moyen en Aquitaine septentrionale : complexité, complémentarité des productions de débitage et de *façonnage* et implications comportementales. Transitions, ruptures et continuité durant la Préhistoire. In: Jaubert, J., Fourment et, N., Depaepe, P. (Eds.), Actes du XXVIIe Congrès Préhistorique de France, Bordeaux – Les Eyzies, 31 mai – 5 juin 2010. Session : Emergence et diversité des techno-complexes au Paléolithique moyen ancien. Relations entre productions de débitage et de *façonnage*.
Brennan, B.J., Lyons, R.G., Phillips, S.W., 1991. Attenuation of alpha particle track dose for spherical grains. Nucl. Tracks Radiat. Meas. 18, 249–253.
Buylaert, J.P., Murray, A.S., Thomsen, K.J., Jain, M., 2009. Testing the potential of an elevated temperature IRSL signal from K-feldspar. Radiat. Meas. 44, 560–565.
Claud, E., 2008. Le statut fonctionnel des bifaces au Paléolithique moyen récent dans le Sud-Ouest de la France. Étude tracéologique intégrée des outillages des sites de La Graulet, La Conne de Bergerac, Combe Brune 2, Fonseigner et Chez-Pinaud/Jonzac. Université de Bordeaux 1, p. 546.

Duttine, M., Guibert, P., Perraut, A., Lahaye, C., Bechtel, F., Villeneuve, G., 2005. Effects of thermal treatment onTL and EPR of flints and their importance in TL-dating: application to French Mousterian sites of Les Forêts (Dordogne) and Jiboui (Drôme). Radiat. Meas. 39, 375–385.
Fain, J., Soumana, S., Montret, M., Pilleyre, T., Sanzelle, S., 1999. Luminescence and ESR dating: beta-dose attenuation for various grain shapes calculated by a Monte-Carlo method. Quat. Geochronol. 18, 231–234.
Guérin, G., Mercier, N., 2011. Determining gamma dose rates by field gamma spectroscopy in sedimentary media: results of Monte Carlo simulations. Radiat. Meas. 46, 190–195.
Guérin, G., Discamps, E., Lahaye, C., Mercier, N., Guibert, P., Turq, A., Dibble, H.L., McPherron, S.P., Sandgathe, D., Goldberg, P., Jain, M., Thomsen, K., Patou-Mathis, M., Castel, J.-C., Soulier, M.-C., 2012. Multi-method (TL and OSL), multi-material (quartz and flint) dating of the Mousterian site of Roc de Marsal (Dordogne, France): correlating Neanderthal occupations with the climatic variability of MIS 5-3. J. Archaeol. Sci. 39, 3071–3084.
Guibert, P., Lahaye, C., Bechtel, F., 2009. The importance of U-series disequilibrium of sediments in luminescence dating: a case study at the Roc de Marsal Cave (Dordogne, France). Radiat. Meas. 44, 223–231.
Guibert, P., Schvoerer, M., 1991. TL dating: low background gamma spectrometry as a tool for the determination of the annual dose. Nucl. Tracks Radiat. Meas. 18, 231–238.
Guibert, P., Vartanian, E., Bechtel, F., Schvoerer, M., 1996. Non-linear approach of TL response to dose: polynomial approximation. Anc. TL 14, 7–14.
Haessaerts, P., Mestdagh, H., Bosquet, D., 1999. The sequence of Remicourt (Hesbaye, Belgium): new insights on the pedo- and chronostratigraphy of the Rocourt soil. Geologica Belgica 2 (3–4), 5–27.
Hernandez, M., 2011. Cadre chronologique des peuplements humains et des paléoenvironnements dans le Sud-Ouest de la France au Pléistocène moyen. In: Apport des datations par luminescence stimulée optiquement, Université Michel de Montaigne Bordeaux 3, Bordeaux, p. 228.
Hernandez, M., Mauz, B., Mercier, N., Shen, Z., 2012. Evaluating the efficiency of TT-OSL SAR protocols. Radiat. Meas. 47, 669–673.
Huntley, D.J., Baril, M.R., 1997. The K content of the K-feldspars being measured in optical dating or in thermoluminescence dating. Anc. TL 15, 11–13.
Huntley, D.J., Lamothe, M., 2001. Ubiquity of anomalous fading in K-feldspars and the measurement and correction for it in optical dating. Can. J. Earth Sci. 38, 1093–1106.
Jain, M., Ankjaergaard, C., 2011. Towards a non-fading signal in feldspar: insight into charge transport and tunnelling from time-resolved optically stimulated luminescence. Radiat. Meas. 46, 292–309.
Lamothe, M., Auclair, M., Hamzaoui, C., Huot, S., 2003. Towards a prediction of long-term anomalous fading of feldspar IRSL. Radiat. Meas. 37, 493–498.
Mejdahl, V., 1979. Thermoluminescence dating: beta dose attenuation in quartz grains. Archaeometry 21, 61–72.
Mercier, N., 1991. Flint palaeodose determination at the onset of saturation, international journal of radiation applications and instrumentation. Part D. Nucl. Tracks Radiat. Meas. 18, 77–79.
Mercier, N., Valladas, H., Valladas, G., 1995a. Flint thermoluminescence dates from the CFR laboratory at Gif: contributions to the study of the chronology of the middle palaeolithic. Quat. Sci. Rev. 14, 351–364.
Mercier, N., Valladas, H., Valladas, G., Reyss, J.-L., Jelinek, A., Meignen, L., Joron, J.L., 1995b. TL dates of burnt flints from Jelinek's excavations at Tabun and their implications. J. Archaeol. Sci. 22, 495–509.
Mercier, N., Valladas, H., Froget, L., Joron, J.L., Reyss, J.L., Balescu, S., Escutenaire, C., Kozlowski, J., Sitlivy, V., Sobczyk, K., Zieba, A., 2003. Luminescence dates for the palaeolithic site of Piekary Ila (Poland): comparison between TL of burnt flints and OSL of a loess-like deposit. Quat. Sci. Rev. 22, 1245–1249.
Mercier, N., Wengler, L., Valladas, H., Joron, J.L., Froget, L., Reyss, J.L., 2007. The Rhafas Cave (Morocco): chronology of the mousterian and aterian archaeological occupations and their implications for quaternary geochronology based on luminescence (TL/OSL) age determinations. Quat. Geochronol. 2, 309–313.
Morthekai, P., Jain, M., Murray, A.S., Thomsen, K.J., Botter-Jensen, L., 2008. Fading characteristics of martian analogue materials and the applicability of a correction procedure. Radiat. Meas. 43, 672–678.
Prescott, J.R., Hutton, J.T., 1994. Cosmic ray contributions to dose rates for luminescence and ESR dating: large depths and long-term time variations. Radiat. Meas. 23, 497–500.
Richter, D., Dibble, H., Goldberg, P., McPherron, S.P., Niven, L., Sandgathe, D., Talamo, S., Turq, A., 2012. The late Middle Palaeolithic in Southwest France: New TL dates for the sequence of Pech de l'Azé IV. Quaternary International.
Schvoerer, M., Gaultier, J., Hauw, C., Mellado, J.M., 1975. Brevet ANVAR / CNRS n °7, 501 189.
Spooner, N.A., 1994. The anomalous fading of infrared-stimulated luminescence from feldspars. Radiat. Meas. 23, 625–632.
Thomsen, K.J., Murray, A.S., Jain, M., Bøtter-Jensen, L., 2008. Laboratory fading rates of various luminescence signals from feldspar-rich sediment extracts. Radiat. Meas. 43, 1474–1486.
Tribolo, C., Mercier, N., Valladas, H., Joron, J.L., Guibert, P., Lefrais, Y., Selo, M., Texier, J.-P., Rigaud, J.-P., Porraz, G., Poggenpoel, C., Parkington, J.E., Texier, J.-P., Lenoble, A., 2009. Thermoluminescence dating of a stillbay howiesons poort sequence at Diepkloof rock shelter (Western Cape, South Africa). J. Archaeol. Sci. 36, 730–739.
Valladas, H., Mercier, N., Froget, L., Joron, J.L., Louis Reyss, J., Aubry, T., 2001. TL dating of upper palaeolithic sites in the Coa Valley (Portugal). Quat. Sci. Rev. 20, 939–943.
Valladas, H., Mercier, N., Joron, J.L., McPherron, S.P., Dibble, H.L., Lenoir, M., 2003. TL dates for the middle paleolithic site of Combe-Capelle Bas, France. J. Archaeol. Sci. 30, 1443–1450.
Valladas, H., Mercier, N., Froget, L., Joron, J.-L., Reyss, J.-L., Karkanas, P., Panagopoulou, E., Kyparissi-Apostolika, N., 2007. TL age-estimates for the middle palaeolithic layers at Theopetra cave (Greece). Quat. Geochronol. 2, 303–308.
Van Vliet-Lanoë, B., 1990. Le pédocomplexe de Warneton: où en est-on ? Bilan paléopédologique et micromorphologique. Quaternaire 1, 65–76.
Visocekas, R., 1979. Miscellaneous aspects of artificial TL of calcite: emission spectra, athermal detrapping and anomalous fading. PACT 3, 258–265.
Wang, X.L., Lu, Y.C., Wintle, A.G., 2006. Recuperated OSL dating of fine-grained quartz in Chinese loess. Quat. Geochronol. 1, 89–100.
Wallinga, J., Bos, A.J.J., Dorenbos, P., Murray, A.S., Schokker, J., 2007. A test case for anomalous fading correction in IRSL dating. Quat. Geochronol. 2, 216–221.
Wintle, A.G., 1997. Luminescence dating: laboratory procedures and protocols. Radiat. Meas. 27, 769–817.
Wintle, A.G., 1973. Anomalous fading of thermoluminescence in mineral samples. Nature 245, 143–144.